

ON ANISOTROPIC DIFFUSION EQUATIONS FOR LABEL PROPAGATION

LISA MARIA KREUSSER AND MARIE-THERESE WOLFRAM

ABSTRACT. In many problems in data classification one wishes to assign labels to points in a point cloud with a certain number of them being already correctly labeled. In this paper, we propose a microscopic ODE approach, in which information about correct labels is propagated to neighboring points. Its dynamics are based on alignment mechanisms, which are often used in collective and consensus models. We derive the respective continuum description, which corresponds to an anisotropic diffusion equation with reaction term. Solutions of the continuum model inherit interesting properties of the underlying point cloud. We discuss these analytic properties and exemplify the results with micro- and macroscopic simulations.

1. INTRODUCTION

Collective dynamics can be observed in many instances of interacting agent systems, such as fish schools, bird flocks or large societies. In these systems imitation, alignment and other interactions lead to the formation of complex patterns and stationary states such as flocks or clusters. This collective and self-organized behavior initiated a lot of research in the applied maths community and inspired the development of many algorithmic in data science, machine learning and robotics. In this paper we will apply ideas from collective dynamics in the context of labeling and classification problems. We wish to assign labels to given set of n data points, some of them being already correctly matched to labels - a situation known as semi-supervised learning. We assume that information about correct labels is then propagated to unlabeled points - using similar interaction rules as in consensus formation or collective dynamics. Hereby interactions depend on the closeness of points - usually particles only interact within a certain radius $\varepsilon > 0$. Let $u_i = u_i(t)$, $i = 1, \dots, n$, denote a characteristic of agent i , for example its opinion, and $w_{ij} = \eta(x_i, x_j, \varepsilon)$ the influence that agent i has on j . Then agents interact via

$$\frac{du_i}{dt} = \sum_{j \neq i} w_{ij}(u_j - u_i) \text{ for } i = 1, \dots, n. \quad (1.1)$$

Several well-known models fall into this category - for example the celebrated Cucker-Smale model, see [4], Krause's opinion formation model, see [12], or consensus formation models in large interacting agent systems, see [17]. Related interacting agent systems with an anisotropic interaction or influence function have only recently been considered, for example in the context of fingerprint formation, see [5].

We will consider (1.1) with an additional regularization term, which enforces binary labels of points through a double well potential. Furthermore we assume that already labeled points only influence others via interaction - a situation similar to interactions with leaders in opinion formation, see [6].

Models of type (1.1) have been used not only in biology, but also in classification and graph-partitioning problems in machine learning. Hereby agents relate to data points or vertices of a weighted graph; the interaction function w_{ij} to the edge weights. The interaction term in (1.1) corresponds to the graph Laplacian - its eigenmaps are used in spectral clustering, which is one of the most popular classes of graph-based clustering methods. Understanding the behavior of eigenvalues and eigenfunctions in suitable scaling limits is therefore of great interest and has been investigated rather recently. First by Trillos and Slepcev for specific choices of the graph Laplacian, see [21], followed by Hoffmann et al. who considered a three-parameter family of graph Laplacians in [11]. In particular Trillos and Slepcev investigate the normalized and unnormalised

graph Laplacian in the context of k clusters by studying the limits of the eigenvectors and eigenvalues. Hereby they consider the simultaneous limit $n \rightarrow \infty$ while the scaling parameter ε in the weights tends to zero. They use the notion of Γ -convergence to analyze the respective Dirichlet energies in suitable function spaces. Hoffmann et al. applied similar techniques to investigate the spectral analysis of a family of weighted graph Laplacians in the situation where the data comprises two nearly separated clusters. In this case, the Fiedler vector - the eigenvector of the second-smallest eigenvalue of the graph Laplacian - is used to partition the graph. They also show that the weighted graph Laplacians converge to the following class of anisotropic elliptic operators for the label distribution u

$$\mathcal{L}(u) = \frac{1}{\rho^p} \nabla \cdot \left(\rho^q \nabla \left(\frac{u}{\rho^r} \right) \right), \quad (1.2)$$

where ρ denotes the distribution of points with parameters $p, q, r \in \mathbb{R}$ fixed.

We will present a formal as well as a rigorous derivation of the limiting continuum model for the proposed microscopic labeling model. The formal approach investigates the behavior of the respective energy functionals, which account for already correctly labeled points and their specific interactions in the simultaneous limit $n \rightarrow \infty$ and $\varepsilon \rightarrow 0$. In the rigorous approach we consider the limiting problem starting from the proposed ODE system instead of the energy functional and hence no analysis of the spectrum is required. In both approaches the derived interaction operators are consistent with (1.2), providing an alternative viewpoint and derivation.

Graph Laplacians in connection with suitable regularization terms have been investigated in various applications in data science and imaging in the last years. For example van Gennip et al. studied the asymptotic behavior of the graph Laplacian and a double well potential, which corresponds to the graph-based formulation of the well-known Allen-Cahn equation, see [9]. Merkurjev et al. [13] used related ideas, presented in [1], to propose computationally efficient algorithms to compute eigenvalues and eigenvectors of graph Laplacians and improve the performance of existing methods, such as the Merriman-Bence-Osher algorithm. We would like to mention that the notion and idea of label propagation was also explored in the machine learning community, see [22, 23].

The contributions of this paper can be summarized as follows:

- (1) *Model development:* We provide a new perspective on label propagation, which connects collective dynamics models in the life sciences with graph-Laplacians in data science. The respective methodologies are well established in their fields, the proposed model adapts them in the context of semi-supervised learning and establishes new connections.
- (2) *Continuum models:* We present an alternative derivation of the respective continuum models using an energy based approach as well as a rigorous mean-field limit.
- (3) *Quantitative behavior:* We present several analytic results to characterize the behavior of solutions to the continuum problem.
- (4) *Computational experiments:* We illustrate and exemplify the structure of solutions to the micro- as well as macroscopic equation with various computational experiments.

This paper is organized as follows. We introduce the microscopic model for label propagation in Section 2, before continuing with the derivation of the macroscopic description from the energy formulation and the rigorous derivation of the mean-field limit in Section 3. We discuss the properties of solutions to the continuum model in Section 4 and conclude with computational experiments in Section 5.

2. DESCRIPTION OF THE DISCRETE MODEL

We start by introducing the proposed label propagation model on the microscopic level. We consider a point cloud

$$V = \{X_1, \dots, X_{n+m}\}$$

of data points X_i in some bounded domain $\Omega \subset \mathbb{R}^d$ for $d \geq 1$ and $m, n \in \mathbb{N}$. In the following, we assume that the first n points X_i for $i = 1, \dots, n$, are not yet labeled, while the points X_i for

$i = n+1, \dots, n+m$ are equipped with labels $L = \{l_1, \dots, l_k\}$ for some $k \ll n$ with $l_1 < \dots < l_k$. We denote the set of points associated to each label by V'_i and assume that $V'_1, \dots, V'_k \subset V$ such that $V'_i \cap V'_j = \emptyset$ for $i, j \in \{1, \dots, k\}$ with $i \neq j$.

We propagate information from close correctly labeled points to neighboring unlabeled ones. This assumption is well established in collective dynamic models, in which interactions depend on the metric or topological distance, see for example [3, 10]. We relate the closeness of two data points to their metric distance and from now on consider the topology of the underlying respective graph G and its weights w . This leads to a weighted graph $G = (V, E, w)$, where V corresponds to the set of data points or agents, E the connecting edges and w the fixed interaction rates or weights. We assume that G is connected, i.e. each vertex is connected to at least another one and hence for each $i \in V$ there exists $j \in V \setminus \{i\}$ such that $w_{ij} \neq 0$. In the following, we also assume that the weights are symmetric, i.e. $w_{ij} = w_{ji}$, and we consider two clusters, i.e. $k = 2$.

Let $\gamma > 0$ and $\kappa > 0$ be given constant and let $W: \mathbb{R} \rightarrow \mathbb{R}$ denote a double well potential with wells at $l_1 = -1$ and $l_2 = 1$, for example $W(x) = (x^2 - 1)^2$. Given a graph G with weights w_{ij} and $V' = V'_1 \cup V'_2$, we assume that labels u_i for $i \in V$ of unlabeled points change according to

$$\frac{du_i}{dt} = \gamma \sum_{j \neq i} w_{ij} (u_j - u_i) - \kappa W'(u_i), \quad i = 1, \dots, n. \quad (2.1)$$

We can extend the sum in (2.1) to the entire set of points V . Therefore

$$\frac{du_i}{dt} = \gamma \sum_{j=1}^{n+m} w_{ij} (u_j - u_i) - \kappa W'(u_i), \quad i = 1, \dots, n.$$

Since we are interested in the large number particle limit, we rescale the amplitude of the interaction term as follows

$$\frac{du_i}{dt} = \frac{\gamma}{n+m} \sum_{j=1}^{n+m} w_{ij} (u_j - u_i) - \kappa W'(u_i), \quad i = 1, \dots, n. \quad (2.2a)$$

Labels of points in V'_1 and V'_2 do not change, but influence the dynamics via the interaction term in (2.2a). Hence the following equalities have to be added to (2.2a)

$$u_i = -1, \quad i \in V'_1, \quad u_i = 1, \quad i \in V'_2. \quad (2.2b)$$

Furthermore we supplement the system with the initial label distribution

$$u_i(0) = -1, \quad i \in V'_1, \quad u_i(0) = 1, \quad i \in V'_2, \quad u_i(0) = 0, \quad i \in V \setminus V'. \quad (2.2c)$$

Then the corresponding energy functional is given by

$$\begin{aligned} E(u_1, \dots, u_n) &= \frac{\gamma}{4n(n+m)} \sum_{i=1}^n \sum_{j=1}^n w_{ij} (u_j - u_i)^2 \\ &\quad + \frac{\gamma}{2n(n+m)} \sum_{i=1}^n \sum_{j=n+1}^{n+m} w_{ij} (u_j - u_i)^2 + \frac{\kappa}{n} \sum_{i=1}^n W(u_i), \end{aligned} \quad (2.3)$$

where we rescaled by n due to the summation over $i = 1, \dots, n$. The slightly unusual form of the energy E stems from dependence of E on u_i for $i = 1, \dots, n$ while u_i for $i = n+1, \dots, n+m$ are fixed by conditions (2.2b).

3. DERIVATION OF THE MACROSCOPIC MODEL

We continue by presenting two different approaches to derive the continuum description in the limit $n \rightarrow \infty$ and $\varepsilon \rightarrow 0$ - the first one is a formal argument based on the energy formulation, while the second one is derived rigorously from the respective ODE system.

Let $\rho \in \mathcal{P}(\Omega)$ denote the distribution of points $V = \{X_1, \dots, X_{n+m}\}$ and $\mathcal{P}(\Omega)$ corresponds to the space of probability measures on Ω . The points $X_1, \dots, X_{n+m} \in \mathbb{R}^d$ define the associated empirical measure $\rho_n(x) = \frac{1}{n+m} \sum_{i=1}^{n+m} \delta_{X_i}(x)$. Furthermore we introduce the function $u: \Omega \rightarrow \mathbb{R}$ satisfying $u(X_i) = u_i$ for all $i = 1, \dots, n+m$. To rescale the discrete weights we consider the

function $\bar{\eta}: \mathbb{R}^d \rightarrow [0, \infty)$. More precisely, we assume that the kernel $\bar{\eta}$ is isotropic and given by the radial profile $\eta: [0, \infty) \rightarrow [0, \infty)$, i.e. $\bar{\eta}(x) = \eta(|x|)$, satisfying

- (1) $\eta(0) > 0$ and η is continuous at 0.
- (2) η is non-increasing.
- (3) $\int_0^\infty \eta(s)s^{d+1} ds < +\infty$.

Due to Assumption (3) and the radial symmetry of η we define

$$\sigma_\eta := \frac{1}{2} \int_{\mathbb{R}^d} \eta(|x|) |x \cdot r|^2 dx < +\infty, \quad (3.1)$$

for any normal vector $r \in \mathbb{R}^d$. Note that the assumptions on η are not restrictive and include a broad class of kernels such as Gaussian kernels and discontinuous kernels like $\eta(s) = \mathbb{1}_{[0, R]}(s)$, where $\mathbb{1}_{[0, R]}$ denotes the indicator function on $[0, R]$ for some $R > 0$. We will later consider the appropriately rescaled function $\eta_\varepsilon(s) = \varepsilon^{-d} \eta(\frac{s}{\varepsilon})$ in the limit. We assume that significant weight is given to edges connecting points up to distance ε and that the weights of the graph are given by $w_{ij} = \eta_\varepsilon(|X_i - X_j|)$. With the limit $n \rightarrow \infty$ in mind, this suggests to consider a given scaling ε with respect to n . In addition, the interaction term in (2.2a) has to be rescaled by ε^2 , resulting in

$$\frac{du_i}{dt} = \frac{\gamma}{\varepsilon^2(n+m)} \sum_{j=1}^{n+m} \eta_\varepsilon(|X_i - X_j|)(u_j - u_i) - \kappa W'(u_i), \quad i = 1, \dots, n, \quad (3.2)$$

while condition (2.2b) implies that

$$\frac{du_i}{dt} = 0, \quad i = n+1, \dots, n+m. \quad (3.3)$$

Similarly, we rescale the interaction term in the energy functional (2.3) by ε^2 which yields

$$\begin{aligned} E_{\varepsilon,n}(u_1, \dots, u_n) &= \frac{\gamma}{4\varepsilon^2 n(n+m)} \sum_{i=1}^n \sum_{j=1}^n \eta_\varepsilon(|X_i - X_j|)(u_j - u_i)^2 \\ &\quad + \frac{\gamma}{2\varepsilon^2 n(n+m)} \sum_{i=1}^n \sum_{j=n+1}^{n+m} \eta_\varepsilon(|X_i - X_j|)(u_j - u_i)^2 + \frac{\kappa}{n} \sum_{i=1}^n W(u_i). \end{aligned} \quad (3.4)$$

Note that (3.2) corresponds to the L^2 gradient flow of the energy (3.4).

3.1. Properties of the discrete system for $\varepsilon > 0$. We continue by discussing the existence of solutions of the discrete system for $\varepsilon > 0$ under the assumption that the initial condition satisfies

$$\sup_{\varepsilon > 0} \sup_{n \in \mathbb{N}} E_{\varepsilon,n}(u_1(0), \dots, u_n(0)) < \infty. \quad (3.5)$$

Note that we will use the shorthand notation $u(t) = (u_1(t), \dots, u_n(t))$ in the following.

Proposition 3.1 *Let $\varepsilon > 0$ and $n \in \mathbb{N}$ be given and suppose that the initial condition satisfies (3.5). Then, the regularized discrete system (3.2) with condition (2.2b) and initial data (2.2c) has a unique solution on $[0, T]$ which is uniformly bounded with respect to $t \in [0, T]$, $n \in \mathbb{N}$ and $\varepsilon > 0$. In particular,*

$$E_{\varepsilon,n}(u_1(t), \dots, u_n(t)) + \frac{1}{n} \sum_{i=1}^n \int_0^t \left(\frac{du_i(s)}{dt} \right)^2 ds = E_{\varepsilon,n}(u_1(0), \dots, u_n(0)). \quad (3.6)$$

Proof. Since $W'(u_i)$ is monotonically increasing in u_i outside the compact interval $[-1, 1]$, Picard Lindelöf ensures the existence of a unique, continuously differentiable solutions to (3.2). The boundedness of the solution follows from an energy identity. Using (3.2) and (3.3), we obtain

$$\frac{d}{dt} E_{\varepsilon,n}(u_1, \dots, u_n) = -\frac{1}{n} \sum_{i=1}^n \left(\frac{du_i}{dt} \right)^2.$$

This yields (3.6). The uniform boundedness of $E_{\varepsilon,n}(u(t))$ with respect to ε and n follows from the uniform boundedness of $E_{\varepsilon,n}(u(0))$. \square

3.2. Energy approach. First we consider the formal limit of the energy functional $E_{\varepsilon,n}$ as $n \rightarrow \infty$ and $\varepsilon \rightarrow 0$, before presenting the rigorous derivation in the next section.

Let (2.2c) satisfy (3.5). Energy (3.4) can be rewritten as

$$E_{\varepsilon,n}(u) = \frac{\gamma}{4\varepsilon^2 n(n+m)} \sum_{i=1}^{n+m} \sum_{j=1}^{n+m} \eta_\varepsilon(|X_i - X_j|)(u_j - u_i)^2 - \frac{\gamma}{4\varepsilon^2 n(n+m)} \sum_{i=n+1}^{n+m} \sum_{j=n+1}^{n+m} \eta_\varepsilon(|X_i - X_j|)(u_j - u_i)^2 + \frac{\kappa}{n} \sum_{i=1}^{n+m} W(u_i)$$

where $W(u_i) = 0$ for $i = n+1, \dots, n+m$ by the definition of W . Since $\frac{1}{n} = \frac{1}{n+m} + \frac{m}{n(n+m)}$, we obtain

$$E_{\varepsilon,n}(u) = \frac{\gamma}{4\varepsilon^2(n+m)^2} \sum_{i=1}^{n+m} \sum_{j=1}^{n+m} \eta_\varepsilon(|X_i - X_j|)(u_j - u_i)^2 + \frac{\kappa}{n+m} \sum_{i=1}^{n+m} W(u_i) + \frac{\kappa m}{n(n+m)} \sum_{i=1}^{n+m} W(u_i) + \frac{\gamma m}{4\varepsilon^2 n(n+m)^2} \sum_{i=1}^{n+m} \sum_{j=1}^{n+m} \eta_\varepsilon(|X_i - X_j|)(u_j - u_i)^2 - \frac{\gamma}{4\varepsilon^2 n(n+m)} \sum_{i=n+1}^{n+m} \sum_{j=n+1}^{n+m} \eta_\varepsilon(|X_i - X_j|)(u_j - u_i)^2.$$

Note that all terms of $E_{\varepsilon,n}$ except the first and second term vanish in the limit $n \rightarrow \infty$ due to the uniform boundedness of u_i . By considering the empirical measure ρ_n and assuming that ρ is bounded in $L^\infty(\Omega)$ as well as $\rho_n \rightarrow \rho$ weakly as $n \rightarrow \infty$, we obtain

$$E_\varepsilon(u) = \lim_{n \rightarrow \infty} E_{\varepsilon,n}(u) = \frac{\gamma}{4} \int_{\Omega} \int_{\Omega} \varepsilon^{-2} \eta_\varepsilon(|y - x|) (u(y) - u(x))^2 \rho(x) \rho(y) dy dx + \kappa \int_{\Omega} W(u(x)) \rho(x) dx. \quad (3.7)$$

Since Ω is a bounded domain, the set $\frac{\Omega - x}{\varepsilon}$ for $x \in \Omega$ contains a neighborhood of the origin whose diameter increases as $\varepsilon > 0$ decreases. We recall that the radially symmetric mollifier η has a compact support, given by the ball $B_r(0)$ for some $r > 0$. In particular, for $x \in \Omega$ given, there exists $\varepsilon_0(x) > 0$ such that $B_r(0) \subset \frac{\Omega - x}{\varepsilon}$ for any $\varepsilon \in (0, \varepsilon_0(x))$. Using a change of variable, we can consider the limit $\varepsilon \rightarrow 0$ of the first term in (3.7):

$$\begin{aligned} & \lim_{\varepsilon \rightarrow 0} \frac{\gamma}{4} \int_{\Omega} \int_{\Omega} \varepsilon^{-2} \eta_\varepsilon(|y - x|) (u(y) - u(x))^2 \rho(x) \rho(y) dy dx \\ &= \lim_{\varepsilon \rightarrow 0} \frac{\gamma}{4} \int_{\Omega} \int_{\frac{\Omega - x}{\varepsilon} \cap B_r(0)} \eta(|z|) \left(\frac{u(x + \varepsilon z) - u(x)}{\varepsilon} \right)^2 \rho(x) \rho(x + \varepsilon z) dz dx \\ &= \frac{\gamma}{4} \int_{\Omega} \int_{B_r(0)} \eta(|z|) (\nabla u(x) \cdot z)^2 \rho^2(x) dz dx \\ &= \frac{\gamma}{4} \sum_{i=1}^d \int_{\Omega} \int_{B_r(0)} \eta(|z|) (\partial_{x_i} u(x))^2 z_i^2 \rho^2(x) dz dx = \frac{\gamma \sigma_\eta}{2} \int_{\Omega} \rho^2(x) |\nabla u(x)|^2 dx, \end{aligned}$$

where we used that the integral of an odd function on a symmetric domain vanishes in the second to the last equality and definition of σ_η (3.1) in the last. Then the resulting limiting energy is given by

$$\mathcal{E}(u) = \frac{\gamma \sigma_\eta}{2} \int_{\Omega} \rho^2 |\nabla u|^2 dx + \kappa \int_{\Omega} \rho W(u) dx. \quad (3.8)$$

Its associated L^2 -gradient flow is given by

$$\partial_t u = \gamma \sigma_\eta \nabla \cdot (\rho^2 \nabla u) - \kappa \rho W'(u), \quad x \in \Omega \setminus V'.$$

This PDE can be rewritten as

$$\partial_t u = \rho (\gamma \sigma_\eta (\rho \nabla^2 u + 2 \nabla \rho \nabla u) - \kappa W'(u)), \quad x \in \Omega \setminus V'.$$

An anisotropic rescaling in time, assuming that the density $\rho \in L^\infty(\Omega)$ is bounded from below by a positive constant, yields

$$\partial_t u = \gamma \sigma_\eta (\rho \nabla^2 u + 2 \nabla \rho \nabla u) - \kappa W'(u), \quad x \in \Omega \setminus V',$$

which is equivalent to

$$\partial_t (\rho u) = \rho \partial_t u = \gamma \sigma_\eta \nabla \cdot (\rho^2 \nabla u) - \kappa \rho W'(u), \quad x \in \Omega \setminus V'. \quad (3.9)$$

Note that the anisotropic diffusion operator in (3.9) is given by

$$\mathcal{L}(u) = \frac{1}{\rho} \nabla \cdot (\rho^2 \nabla u) \quad (3.10)$$

which agrees with the derived differential operator, when studying the spectral properties of the graph Laplacian in the large data limit, see [11]. Operator (3.10) corresponds to the choice $(p, q, r) = (1, 2, 0)$ in (1.2), which is obtained from the unnormalised graph Laplacian. We recall that the Fiedler vector, that is the eigenvector of the second-smallest eigenvalue of (3.10), is used for classification. In our case it is not clear how the additional regularization term effects the Fiedler vector - a question which we plan to investigate in the future.

3.3. Rigorous mean-field limit. Next, we analyze the limiting behavior of weak solutions to (3.2) as $n \rightarrow \infty$ and $\varepsilon \rightarrow 0$, assuming that (3.5) is satisfied.

For every test function $\phi \in C^1(\Omega)$ we have

$$\begin{aligned} \frac{d}{dt} \int_{\Omega} \phi \rho_n u \, dx &= \frac{1}{n+m} \sum_{i=1}^{n+m} \phi(X_i) \frac{d}{dt} u(X_i) \\ &= \frac{1}{n+m} \sum_{i=1}^{n+m} \phi(X_i) \left(\frac{\gamma}{\varepsilon^2(n+m)} \sum_{j=1}^{n+m} \eta_\varepsilon(|X_i - X_j|)(u_j - u_i) - \kappa W'(u_i) \right) \\ &\quad - \frac{1}{n+m} \sum_{i=n+1}^{n+m} \phi(X_i) \left(\frac{\gamma}{\varepsilon^2(n+m)} \sum_{j=1}^{n+m} \eta_\varepsilon(|X_i - X_j|)(u_j - u_i) \right), \end{aligned}$$

where we used (3.3) and that $W'(u_i) = 0$ for $i = n+1, \dots, n+m$. The second term vanishes in the limit as $n \rightarrow \infty$ since the function u_i is uniformly bounded with respect to n , see Proposition 3.1. The first term can be written as

$$\frac{\gamma}{\varepsilon^2} \int_{\Omega} \int_{\Omega} \phi(x) \rho_n(x) \rho_n(y) \eta_\varepsilon(|x - y|)(u(y) - u(x)) \, dy \, dx - \kappa \int_{\Omega} \phi(x) \rho_n(x) W'(u(x)) \, dx.$$

This yields

$$\begin{aligned} \frac{d}{dt} \int_{\Omega} \phi \rho u \, dx &= \lim_{n \rightarrow \infty} \frac{d}{dt} \int_{\Omega} \phi \rho_n u \, dx \\ &= \frac{\gamma}{\varepsilon^2} \int_{\Omega} \int_{\Omega} \phi(x) \rho(x) \rho(y) \eta_\varepsilon(|x - y|)(u(y) - u(x)) \, dy \, dx \\ &\quad - \kappa \int_{\Omega} \phi(x) \rho(x) W'(u(x)) \, dx, \end{aligned} \quad (3.11)$$

where we used that $\rho_n \rightarrow \rho$ weakly as $n \rightarrow \infty$ and Proposition 3.1. Note that it is sufficient to study the limit $\varepsilon \rightarrow 0$ of the first term in (3.11) only. We use the same change of variables as in Section 3.2 and rewrite the first term on the right-hand side of (3.11) as (for $\varepsilon > 0$ sufficiently small):

$$\frac{\gamma}{\varepsilon^2} \int_{\Omega} \int_{B_r(0)} \phi(x) \rho(x) \rho(x + \varepsilon z) \eta(|z|)(u(x + \varepsilon z) - u(x)) \, dz \, dx. \quad (3.12)$$

For the ease of notation, we assume that $\rho \in C^1(\Omega)$. However, the arguments can be extended to $\rho \in L^\infty(\Omega)$ by introducing a regularization of ρ , defined by $\rho * \xi_\delta$ for a non-negative, radially

symmetric mollifier ξ_δ with $\delta > 0$, and considering the limit as $\delta \rightarrow 0$. For $z = (z_1, \dots, z_d)$, it holds

$$u(x + \varepsilon z) - u(x) = \sum_{i=1}^d \left(u(x + \varepsilon \sum_{j=1}^i z_j e_j) - u(x + \varepsilon \sum_{j=1}^{i-1} z_j e_j) \right),$$

where e_j denotes the j th orthonormal basis vector of the d -dimensional Euclidean space. Note that any $z \in B_r(0)$ satisfies $z_j \in Q_{j-1}$ for $j = 1, \dots, d$, where Q_{j-1} is the symmetric interval $Q_j = [-p_j, p_j]$ with $p_j = p_j(z_1, \dots, z_j)$ defined as $p_j = \sqrt{(r^2 - \sum_{i=1}^j z_i^2)}$. Then, the first term of the right-hand side of (3.11) is given by

$$\begin{aligned} & \frac{\gamma}{\varepsilon^2} \int_{\Omega} \int_{\Omega} \phi(x) \rho(x) \rho(y) \eta_\varepsilon(|x - y|) (u(y) - u(x)) \, dy \, dx \\ &= \frac{\gamma}{\varepsilon^2} \sum_{i=1}^d \int_{\Omega} \int_{Q_0} \cdots \int_{Q_{d-1}} \phi(x) \rho(x) \rho(x + \varepsilon z) \eta(|z|) \\ & \quad \cdot \left(u(x + \varepsilon \sum_{j=1}^i z_j e_j) - u(x + \varepsilon \sum_{j=1}^{i-1} z_j e_j) \right) \, dz_d \cdots \, dz_1 \, dx. \end{aligned} \quad (3.13)$$

For the sake of readability, we consider some fixed $i \in \{1, \dots, d\}$ and consider only the i th summand for now. Then, the integral over Q_{i-1} with respect to z_i is given by

$$\frac{\gamma}{\varepsilon^2} \int_{Q_{i-1}} \phi(x) \rho(x) \rho(x + \varepsilon z) \eta(|z|) \left(u(x + \varepsilon \sum_{j=1}^i z_j e_j) - u(x + \varepsilon \sum_{j=1}^{i-1} z_j e_j) \right) \, dz_i. \quad (3.14)$$

Replacing $\rho(x + \varepsilon z)$ by $\rho(x) + (\rho(x + \varepsilon z) - \rho(x))$ allows us to write (3.14) as the sum of two terms. For the first term, we have

$$\begin{aligned} & \frac{\gamma}{\varepsilon^2} \int_{Q_{i-1}} \phi(x) \rho^2(x) \eta(|z|) \left(u(x + \varepsilon \sum_{j=1}^i z_j e_j) - u(x + \varepsilon \sum_{j=1}^{i-1} z_j e_j) \right) \, dz_i \\ &= \gamma \int_0^{p_{i-1}} \phi(x) \rho^2(x) \eta(|z|) z_i^2 \frac{u(x + \varepsilon \sum_{j=1}^{i-1} z_j e_j + \varepsilon z_i e_i) - u(x + \varepsilon \sum_{j=1}^{i-1} z_j e_j)}{\varepsilon^2 z_i^2} \, dz_i \\ &+ \gamma \int_0^{p_{i-1}} \phi(x) \rho^2(x) \eta(|z|) z_i^2 \frac{u(x + \varepsilon \sum_{j=1}^{i-1} z_j e_j - \varepsilon z_i e_i) - u(x + \varepsilon \sum_{j=1}^{i-1} z_j e_j)}{\varepsilon^2 z_i^2} \, dz_i. \end{aligned}$$

It converges to

$$\gamma \int_0^{p_{i-1}} \phi(x) \rho^2(x) \eta(|z|) z_i^2 \partial_{x_i}^2 u(x) \, dz_i$$

in the limit $\varepsilon \rightarrow 0$. The second term is given by

$$\frac{\gamma}{\varepsilon^2} \int_{Q_{i-1}} \phi(x) \rho(x) ((\rho(x + \varepsilon z) - \rho(x)) \eta(|z|)) \left(u(x + \varepsilon \sum_{j=1}^i z_j e_j) - u(x + \varepsilon \sum_{j=1}^{i-1} z_j e_j) \right) \, dz_i.$$

Using

$$\rho(x + \varepsilon z) - \rho(x) = \sum_{k=1}^d \left(\rho(x + \varepsilon \sum_{l=1}^k z_l e_l) - \rho(x + \varepsilon \sum_{l=1}^{k-1} z_l e_l) \right),$$

we can write it as

$$\begin{aligned} & \sum_{k=1}^d \frac{\gamma}{\varepsilon^2} \int_{Q_{i-1}} \phi(x) \rho(x) \frac{\rho(x + \varepsilon \sum_{l=1}^k z_l e_l) - \rho(x + \varepsilon \sum_{l=1}^{k-1} z_l e_l)}{z_k} \eta(|z|) z_k z_i \\ & \quad \frac{u(x + \varepsilon \sum_{j=1}^{i-1} z_j e_j + \varepsilon z_i e_i) - u(x + \varepsilon \sum_{j=1}^{i-1} z_j e_j)}{z_i} \, dz_i. \end{aligned} \quad (3.15)$$

Due to the symmetry of $Q_{i-1} = [-p_{i-1}, p_{i-1}]$, we split the integral into two. Note that all summands except for the i th vanish in the limit $\varepsilon \rightarrow 0$ since for $k = 1, \dots, i-1$, we have

$$\begin{aligned} \lim_{\varepsilon \rightarrow 0} \left(\frac{\gamma}{\varepsilon^2} \int_0^{p_{i-1}} \phi(x) \rho(x) \frac{\rho(x + \varepsilon \sum_{l=1}^k z_l e_l) - \rho(x + \varepsilon \sum_{l=1}^{k-1} z_l e_l)}{z_k} \eta(|z|) z_k z_i \right. \\ \left(\frac{u(x + \varepsilon \sum_{j=1}^{i-1} z_j e_j + \varepsilon z_i e_i) - u(x + \varepsilon \sum_{j=1}^{i-1} z_j e_j)}{z_i} \right. \\ \left. \left. - \frac{u(x + \varepsilon \sum_{j=1}^{i-1} z_j e_j) - u(x + \varepsilon \sum_{j=1}^{i-1} z_j e_j - \varepsilon z_i e_i)}{z_i} \right) dz_i \right) = 0, \end{aligned}$$

while for $k = i+1, \dots, n$, we obtain

$$\begin{aligned} \lim_{\varepsilon \rightarrow 0} \left(\frac{\gamma}{\varepsilon^2} \int_0^{p_{i-1}} \phi(x) \rho(x) \frac{\rho(x + \varepsilon \sum_{l=1}^k z_l e_l) - \rho(x + \varepsilon \sum_{l=1}^{k-1} z_l e_l)}{z_k} \eta(|z|) z_k z_i \right. \\ \left. \frac{u(x + \varepsilon \sum_{j=1}^{i-1} z_j e_j + \varepsilon z_i e_i) - u(x + \varepsilon \sum_{j=1}^{i-1} z_j e_j)}{z_i} \right. \\ \left. - \phi(x) \rho(x) \frac{\rho(x + \varepsilon \sum_{l=1, l \neq i}^k z_l e_l - \varepsilon z_i e_i) - \rho(x + \varepsilon \sum_{l=1, l \neq i}^{k-1} z_l e_l - \varepsilon z_i e_i)}{z_k} \right. \\ \left. \frac{u(x + \varepsilon \sum_{j=1}^{i-1} z_j e_j) - u(x + \varepsilon \sum_{j=1}^{i-1} z_j e_j - \varepsilon z_i e_i)}{z_i} dz_i \right) \\ = \gamma \int_0^{p_{i-1}} \phi(x) \rho(x) (\partial_{x_k} \rho(x) \eta(|z|) z_k z_i \partial_{x_i} u(x) - \partial_{x_k} \rho(x) \eta(|z|) z_k z_i \partial_{x_i} u(x)) dz_i = 0. \end{aligned}$$

The limit of the i th summand in (3.15) as $\varepsilon \rightarrow 0$ is given by

$$\begin{aligned} \lim_{\varepsilon \rightarrow 0} \left(\frac{\gamma}{\varepsilon^2} \int_0^{p_{i-1}} \phi(x) \rho(x) \frac{\rho(x + \varepsilon \sum_{l=1}^i z_l e_l) - \rho(x + \varepsilon \sum_{l=1}^{i-1} z_l e_l)}{z_i} \eta(|z|) z_i^2 \right. \\ \left. \frac{u(x + \varepsilon \sum_{j=1}^{i-1} z_j e_j + \varepsilon z_i e_i) - u(x + \varepsilon \sum_{j=1}^{i-1} z_j e_j)}{z_i} \right. \\ \left. + \phi(x) \rho(x) \frac{\rho(x + \varepsilon \sum_{l=1}^{i-1} z_l e_l - \varepsilon z_i e_i) - \rho(x + \varepsilon \sum_{l=1}^{i-1} z_l e_l)}{z_i} \eta(|z|) z_i^2 \right. \\ \left. \frac{u(x + \varepsilon \sum_{j=1}^{i-1} z_j e_j - \varepsilon z_i e_i) - u(x + \varepsilon \sum_{j=1}^{i-1} z_j e_j)}{z_i} dz_i \right) \\ = 2\gamma \int_0^{p_{i-1}} \phi(x) \rho(x) \partial_{x_i} \rho(x) \eta(|z|) z_i^2 \partial_{x_i} u(x) dz_i. \end{aligned}$$

Combining all of the above gives

$$\begin{aligned} \lim_{\varepsilon \rightarrow 0} \frac{\gamma}{\varepsilon^2} \int_{Q_{i-1}} \phi(x) \rho(x) \rho(x + \varepsilon z) \eta(|z|) \left(u(x + \varepsilon \sum_{j=1}^i z_j e_j) - u(x + \varepsilon \sum_{j=1}^{i-1} z_j e_j) \right) dz_i \\ = (\gamma \phi(x) \rho^2(x) \partial_{x_i}^2 u(x) + 2\gamma \phi(x) \rho(x) \partial_{x_i} \rho(x) \partial_{x_i} u(x)) \int_0^{p_{i-1}} \eta(|z|) z_i^2 dz_i. \end{aligned}$$

We still need to consider the integrals over Ω and Q_{j-1} for $j \in \{1, \dots, d\} \setminus \{i\}$ with respect to x and z_j , respectively, in addition to the integral over Q_{i-1} . We sum over all $i = 1, \dots, d$ as in (3.13)

and obtain

$$\begin{aligned}
& \lim_{\varepsilon \rightarrow 0} \frac{\gamma}{\varepsilon^2} \int_{\Omega} \int_{\Omega} \phi(x) \rho(x) \rho(y) \eta_{\varepsilon}(|x - y|) (u(y) - u(x)) dy dx \\
&= \sigma_{\eta} \sum_{i=1}^d \int_{\Omega} \gamma \phi(x) \rho^2(x) \partial_{x_i}^2 u(x) + 2\gamma \phi(x) \rho(x) \partial_{x_i} \rho(x) \partial_{x_i} u(x) dx \\
&= \sigma_{\eta} \left(\gamma \int_{\Omega} \phi(x) \rho^2(x) \nabla^2 u(x) dx + 2\gamma \int_{\Omega} \phi(x) \rho(x) \nabla \rho(x) \cdot \nabla u(x) dx \right) \\
&= \gamma \sigma_{\eta} \int_{\Omega} \phi(x) \nabla \cdot (\rho^2(x) \nabla u(x)) dx,
\end{aligned}$$

where we used that σ_{η} is defined independently of $i \in \{1, \dots, d\}$ in (3.1)

$$\int_{Q_0} \cdots \int_{Q_{i-2}} \int_0^{p_{i-1}} \int_{Q_{i+1}} \cdots \int_{Q_d} \eta(|z|) z_i^2 dz_d \cdots dz_1 = \frac{1}{2} \int_{\mathbb{R}^d} \eta(|z|) z_i^2 dz = \sigma_{\eta}.$$

This limiting expression allows us to state the weak formulation (3.11) in the limit $\varepsilon \rightarrow 0$:

$$\frac{d}{dt} \int_{\Omega} \phi \rho u dx = \gamma \sigma_{\eta} \int_{\Omega} \phi(x) \nabla \cdot (\rho^2(x) \nabla u(x)) dx - \kappa \int_{\Omega} \phi(x) \rho(x) W'(u(x)) dx.$$

The associated mean-field PDE is given by

$$\partial_t(\rho u) = \rho \partial_t u = \gamma \sigma_{\eta} \nabla \cdot (\rho^2 \nabla u) - \kappa \rho W'(u)$$

which is identical to (3.9), derived in Section 3.2.

3.4. Initial and boundary conditions. Next we discuss the corresponding initial and boundary conditions to obtain a well-posed problem. We prescribe an initial data u_0 , which corresponds to the discrete interpolation of the microscopic initial condition (2.2c), that is

$$u(x, 0) = u_0(x) \quad x \in \Omega. \quad (3.16)$$

For $t > 0$ and $x \in \partial\Omega \cup V'$, we extend the discrete boundary conditions (2.2b) by considering either Dirichlet or Neumann boundary conditions, as appropriate:

$$u(x, t) = -1, \quad x \in V'_1, \quad u(x, t) = 1, \quad x \in V'_2, \quad \frac{\partial u}{\partial r}(x, t) = 0, \quad x \in \partial\Omega \setminus V'. \quad (3.17)$$

These boundary conditions impose restrictions on the sets V'_1 and V'_2 . In 1D one can solve equation (3.9) on intervals. The intervals are defined by the labeled points at which the respective boundary conditions (3.17) are imposed. In higher dimensions they impose the following additional assumptions:

Assumption 3.2. Suppose that there exists a $p \in \mathbb{N}$ and domains $\Omega_1, \dots, \Omega_p \subset \Omega$ for $p \geq 1$ with $\Omega_i \cap \Omega_j = \emptyset$ for $i \neq j$ such that u is prescribed on $\mathcal{A} = \bar{\Omega} \setminus \cup_{i=1}^p \Omega_i \supset V'$. That is, the labels are consistent, i.e. there exist non-empty sets $\mathcal{A}_1, \mathcal{A}_2 \subset \mathcal{A}$ such that $\mathcal{A}_1 \supset V'_1$ and $\mathcal{A}_2 \supset V'_2$ with $\bar{\mathcal{A}}_1 \cap \bar{\mathcal{A}}_2 = \emptyset$ and $\mathcal{A}_1 \cup \mathcal{A}_2 \cup \partial\Omega = \mathcal{A}$ such that

$$u(x, t) = -1, \quad x \in \mathcal{A}_1, \quad u(x, t) = 1, \quad x \in \mathcal{A}_2, \quad \frac{\partial u}{\partial x}(x, t) = 0, \quad x \in \partial\Omega \setminus (\mathcal{A}_1 \cup \mathcal{A}_2). \quad (3.18)$$

Note that Assumption 3.2 imposes necessary conditions for the continuity of u , in particular that for any $x \in \mathcal{A}_1$ there exists an $r_1 > 0$ such that $B_{r_1}(x) \cap \mathcal{A}_2 = \emptyset$ and for any $x \in \mathcal{A}_2$ there exists an $r_2 > 0$ such that $B_{r_2}(x) \cap \mathcal{A}_1 = \emptyset$. An example of a domain, satisfying Assumption 3.2 is shown in Figure 1. Assumption 3.2 includes the case when all labeled points are in $\partial\Omega$. Then (3.18) corresponds to mixed Dirichlet and Neumann boundary conditions on $\partial\Omega$. For the ease of notation, we introduce the open set $\mathcal{D} = \cup_{i=1}^p \Omega_i \subset \Omega$ for $\Omega_1, \dots, \Omega_p \subset \Omega$ in Assumption 3.2. and consider the PDE (3.9) on \mathcal{D} only, i.e.

$$\partial_t(\rho u) = \rho \partial_t u = \gamma \sigma_{\eta} \nabla \cdot (\rho^2 \nabla u) - \kappa \rho W'(u), \quad x \in \mathcal{D}. \quad (3.19)$$

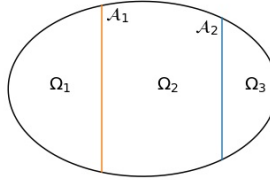


FIGURE 1. Example of domain satisfying Assumption 3.2.

The respective energy (3.8) is then given by

$$\mathcal{E}(u) = \frac{\gamma\sigma\eta}{2} \int_{\mathcal{D}} \rho^2 |\nabla u|^2 \, dx + \kappa \int_{\mathcal{D}} \rho W(u) \, dx. \quad (3.20)$$

In summary we can formulate the continuum problem as follows: Let ρ be a given probability measure, that is $\int_{\mathcal{D}} \rho \, dx = 1$, satisfying $\rho(X_i) > 0$ for all $i \in V'$. Then continuous label propagation can be described by (3.19) with initial condition (3.16) for a smooth initial label distribution obtained by the interpolation of (2.2c) and boundary conditions (3.17).

3.5. Extension to multiple labels. We briefly comment on multi-label problems, before returning to the case of two labels in Section 4. For multiple labels we consider $L = \{l_1, \dots, l_k\}$ and the set of initially labeled vertices $V' = V'_1 \cup \dots \cup V'_k$ where $V'_i \cap V'_j = \emptyset$ for $i, j \in \{1, \dots, k\}$ with $i \neq j$. The discrete boundary conditions (2.2b) can be adapted as

$$u_i = l_1, \quad i \in V'_1, \quad \dots, \quad u_i = l_k, \quad i \in V'_k.$$

This motivates to generalize Assumption 3.2 for k labels:

Assumption 3.3. Suppose that there exists a $p \in \mathbb{N}$ and domains $\Omega_1, \dots, \Omega_p \subset \Omega$ for $p \geq 1$ with $\Omega_i \cap \Omega_j = \emptyset$ for $i \neq j$ such that u is prescribed on $\mathcal{A} = \bar{\Omega} \setminus \cup_{i=1}^p \Omega_i \supset V'$. That is, the labels are consistent, i.e. there exist non-empty sets $\mathcal{A}_1, \dots, \mathcal{A}_k \subset \mathcal{A}$ such that $\mathcal{A}_i \supset V'_i$ for $i = 1, \dots, k$ with $\mathcal{A}_i \cap \mathcal{A}_j = \emptyset$ for any $i \neq j$ and $\mathcal{A}_1 \cup \dots \cup \mathcal{A}_k \cup \partial\Omega = \mathcal{A}$ such that

$$u(x, t) = l_i, \quad x \in \mathcal{A}_i, \quad i = 1, \dots, k, \quad \frac{\partial u}{\partial r}(x, t) = 0, \quad x \in \partial\Omega \setminus (\cup_{i=1}^k \mathcal{A}_i).$$

Note that Assumption 3.3 implies that necessary conditions for the continuity of u are satisfied, i.e. for any $i \in \{1, \dots, k\}$ and any $x \in \mathcal{A}_i$ there exists an $r_i > 0$ such that $B_{r_i}(x) \cap \mathcal{A}_j = \emptyset$ for all $j \in \{1, \dots, k\} \setminus \{i\}$.

4. PROPERTIES OF SOLUTIONS OF THE CONTINUUM MODEL

In this section we present analytic properties of solutions to the continuum model. These results provide insights how the structure of solutions depends on the function ρ and the scaling parameters γ and κ .

Throughout this section we will suppose that Assumption 3.2 is satisfied and denote by $\mathcal{D} = \cup_{i=1}^p \Omega_i \subset \Omega$ an open set, where $\Omega_1, \dots, \Omega_p \subset \Omega$. Furthermore we assume:

- (A1) Let the density $\rho \in L^\infty(\mathcal{D})$ with $\int_{\mathcal{D}} \rho \, dx = 1$ and $\rho(x) \geq \bar{\rho} > 0$.
- (A2) The initial datum $u_0 \in H^1(\Omega)$ satisfies $\mathcal{E}(u_0) < \infty$ for \mathcal{E} given by (3.20).
- (A3) Let $\kappa \geq 0$.

Further, we assume that the double well potential $W: \mathbb{R} \rightarrow [0, \infty)$ satisfies the following assumptions:

- (H1) W is continuously differentiable, $W(t) = 0$ if and only if $t \in \{-1, 1\}$.
- (H2) There exist $c > 0$ and $T_c > 0$ such that $W(t) \geq c|t|$ for all $t \in \mathbb{R}$ with $|t| \geq T_c$.

For the maximum principle, we assume in addition:

- (H3) $W'(t) \leq 0$ for all $t \leq -1$ and $W'(t) \geq 0$ for all $t \geq 1$.

An example for W is $W(x) = (x^2 - 1)^2$.

4.1. Existence and uniqueness of solution.

Theorem 4.1 *Let assumptions 3.2, (A1), (A2), (A3), (H1) and (H2) be satisfied. Then, (3.19) subject to initial data (3.16) and boundary conditions (3.18) has a unique weak solution $u \in L^2(0, \infty; H^1(\mathcal{D}))$. The solution satisfies the energy dissipation inequality*

$$\mathcal{E}(u(t)) + \int_0^t \int_{\mathcal{D}} (\partial_t u(x, s))^2 dx ds \leq \mathcal{E}(u_0) \quad \text{for all } t \geq 0. \quad (4.1)$$

For the proof of the above theorem, we introduce a regularization of (3.19), given by the regularized PDE for $\delta > 0$:

$$(\rho * \xi_\delta) \partial_t u = \gamma \sigma_\eta \nabla \cdot ((\rho * \xi_\delta)^2 \nabla u) - \kappa (\rho * \xi_\delta) W'(u), \quad x \in \mathcal{D}, \quad (4.2)$$

where ξ_δ is a non-negative, radially symmetric mollifier. Moreover, (4.2) is the formal L^2 -gradient flow of the energy

$$\mathcal{E}_\delta(u) = \frac{\gamma \sigma_\eta}{2} \int_{\mathcal{D}} (\rho * \xi_\delta)^2 |\nabla u|^2 dx + \kappa \int_{\mathcal{D}} (\rho * \xi_\delta) W(u) dx. \quad (4.3)$$

Lemma 4.2 *Let Assumptions 3.2, (A1), (A2), (A3), (H1) and (H2) be satisfied and let $\delta > 0$. Then, the regularized PDE (4.2) subject to initial data (3.16) and boundary conditions (3.18) has a unique weak solution $u \in L^2(0, \infty; H^1(\mathcal{D}))$. The regularized energy (4.3) satisfies*

$$\mathcal{E}_\delta(u(t)) + \int_0^t \int_{\mathcal{D}} (\partial_t u(x, s))^2 dx ds = \mathcal{E}_\delta(u_0) \quad \text{for all } t \geq 0. \quad (4.4)$$

Proof. The PDE (4.2) with boundary conditions (3.18) can be regarded as multiple boundary value problems by splitting the given set \mathcal{D} into subdomains $\Omega_1, \dots, \Omega_p$ according to (3.18). Note that the sequence $\{\rho * \xi_\delta\}_{\delta > 0}$ is continuously differentiable and uniformly bounded by a positive constant from below. The term $(\rho * \xi_\delta) W'(u)$ is monotonically increasing in u outside the compact set $[-T_c, T_c]$ by (H2). Hence, (4.2) has at least one solution global in time on \mathcal{D} for any $\kappa \geq 0$ by the classical existence and uniqueness theory of second order parabolic PDEs [7, § 7.2]. The condition $\bar{\mathcal{A}}_1 \cap \bar{\mathcal{A}}_2 = \emptyset$ together with the boundary conditions (3.18) in Assumption 3.2 implies the uniqueness of solutions. To obtain the energy identity (4.4), we integrate by parts

$$\begin{aligned} \frac{d}{dt} \mathcal{E}_\delta(u) &= \gamma \sigma_\eta \int_{\mathcal{D}} (\rho * \xi_\delta)^2 \nabla u \cdot \nabla (\partial_t u) dx + \kappa \int_{\mathcal{D}} (\rho * \xi_\delta) \partial_t u W'(u) dx \\ &= - \int_{\mathcal{D}} \partial_t u (\gamma \sigma_\eta \nabla \cdot ((\rho * \xi_\delta)^2 \nabla u) - \kappa (\rho * \xi_\delta) W'(u)) dx = - \int_{\mathcal{D}} (\partial_t u)^2 dx. \end{aligned}$$

Integration in time yields (4.4). \square

Proof of Theorem 4.1. Let $\{u_\delta\}$ be a sequence of weak solutions of (4.2). Since ρ is bounded from below by a positive constant, $\rho * \xi_\delta$ is also bounded from below by a positive constant, provided $\delta > 0$ is chosen sufficiently small. The energy identity (4.4) implies the uniform boundedness of $\|u_\delta\|_{L^4(\mathcal{D})}$ and $\|\nabla u_\delta\|_{L^2(\mathcal{D})}$. Hence, there exists a sub-sequence, again denoted by u_δ , such that we have the weak convergence $u_\delta \rightharpoonup u$ in $H^1(\mathcal{D})$ for some $u \in H^1(\mathcal{D})$ as $\delta \rightarrow 0$. The strong convergence of $\rho * \xi_\delta$ to ρ in $L^2(\mathcal{D})$ implies the weak convergence $(\rho * \xi_\delta) \nabla u_\delta \rightharpoonup \rho \nabla u$. Since $H^1(\mathcal{D})$ is compact in $L^2(\mathcal{D})$ by the Rellich-Kondrachov theorem [7, § 5.7], u_δ also converges strongly to u in $L^2(\mathcal{D})$.

The weak formulation of (4.2) is given by

$$\int_{\mathcal{D}} \phi (\rho * \xi_\delta) \partial_t u_\delta dx = -\gamma \sigma_\eta \int_{\mathcal{D}} \nabla \phi \cdot ((\rho * \xi_\delta)^2 \nabla u_\delta) dx - \kappa \int_{\mathcal{D}} \phi (\rho * \xi_\delta) W'(u_\delta) dx$$

for any test function $\phi \in H^1(\mathcal{D})$. By the above convergence properties, we obtain

$$\int_{\mathcal{D}} \phi \rho \partial_t u dx = -\gamma \sigma_\eta \int_{\mathcal{D}} \nabla \phi \cdot (\rho^2 \nabla u) dx - \kappa \int_{\mathcal{D}} \phi \rho W'(u) dx$$

in the limit $\delta \rightarrow 0$, i.e. u is a weak solution of (3.19).

The energy dissipation (4.1) follows from passing to the limit $\delta \rightarrow 0$ in (4.4) together with the weak lower semicontinuity of the L^2 -norm and $\mathcal{E}_\delta(u_0) \rightarrow \mathcal{E}(u_0)$ as $\delta \rightarrow 0$. \square

4.2. Consistency of labeling. The PDE (3.19) is possibly strongly degenerate unless ρ is bounded by a positive constant from below. To relax the assumptions on ρ , we consider the following regularization of (3.19)

$$\rho \partial_t u = \gamma \sigma_\eta \nabla \cdot ((\varepsilon + \rho^2) \nabla u) - \kappa \rho W'(u), \quad x \in \mathcal{D}, \quad (4.5)$$

where $\varepsilon = \varepsilon(x) \geq \varepsilon_0 > 0$ is a prescribed function that models the background diffusivity. Clearly, (4.5) is uniformly elliptic for any $\rho \in L^\infty(\mathcal{D})$.

Corollary 4.3 *Suppose that Assumption 3.2, (A1), (A2), (A3), (H1) and (H2) hold. Then, (4.5) subject to initial data (3.16) and boundary conditions (3.18) has a unique weak solution $u \in L^2(0, \infty; H^1(\mathcal{D}))$, which satisfies the energy dissipation inequality*

$$\tilde{\mathcal{E}}(u(t)) + \int_0^t \int_{\mathcal{D}} (\partial_t u(x, s))^2 \, dx \, ds \leq \tilde{\mathcal{E}}(u_0) \quad \text{for all } t \geq 0$$

with

$$\tilde{\mathcal{E}}(u) = \frac{\gamma \sigma_\eta}{2} \int_{\mathcal{D}} (r + \rho^2) |\nabla u|^2 \, dx + \kappa \int_{\mathcal{D}} \rho W(u) \, dx. \quad (4.6)$$

Proof. The statement immediately follows from Theorem 4.1. \square

Note that a stationary solution u to (4.5) has a similar structure as the given probability measure $\rho \in L^\infty(\mathcal{D})$, i.e. $\rho = 0$ almost everywhere on some subset $\mathcal{D}_0 \subset \mathcal{D}$ implies $u = 0$ on \mathcal{D}_0 , while $\rho > 0$ and u constant almost everywhere on some set $\mathcal{D}_c \subset \mathcal{D}$ implies $|u| > 0$ almost everywhere on \mathcal{D}_c . Indeed, let $\rho \in L^\infty(\mathcal{D})$ be a probability measure with $\mathcal{D}_0 = \{x \in \mathcal{D} : \rho(x) = 0\} \neq \emptyset$. The weak formulation of (4.5) implies

$$\int_{\mathcal{D}_0} \nabla \phi \cdot \nabla u \, dx = 0,$$

for any test function $\phi \in H^1(\mathcal{D})$. Therefore ∇u is zero almost everywhere on \mathcal{D}_0 . In particular, u is constant almost everywhere on \mathcal{D}_0 , independent of $t \geq 0$. In case of zero initial data (3.16), we have that $\rho = u = 0$ on \mathcal{D}_0 . For the reverse statement, we consider the set $\tilde{\mathcal{D}} = \mathcal{D} \setminus \mathcal{D}_0$ and suppose that $u \in L^2(0, \infty; H^1(\mathcal{D}))$ is a weak stationary solution of (4.5) satisfying $\nabla u = 0$ almost everywhere on some set $\mathcal{D}_c \subset \tilde{\mathcal{D}}$, i.e. u is constant almost everywhere on \mathcal{D}_c . Then, the weak formulation of (4.5) implies that $W'(u) = 0$ almost everywhere on \mathcal{D}_c . Since $\frac{\delta \tilde{\mathcal{E}}}{\delta u} = \rho \partial_t u = 0$ for $\tilde{\mathcal{E}}$ in (4.6), the function u is a minimizer of $\int_{\mathcal{D}_c} \rho W(u) \, dx$ and therefore $u \in \{-1, 1\}$ almost everywhere on \mathcal{D}_c . In particular, u is non-zero almost everywhere on \mathcal{D}_c .

We see that the function u has similar characteristics as ρ - a property which is desirable from a modeling point of view. It also justifies the assumption that ρ is bounded from below by a positive constant.

4.3. Maximum principle. Next, we show that solutions can attain their maximum and minimum on the parabolic boundary only. For the bounded open set $\mathcal{D} \subset \mathbb{R}^d$ we define $\mathcal{D}_T = \mathcal{D} \times (0, T]$ for some fixed time $T > 0$ and $\Gamma = \{(x, t) \in \bar{\mathcal{D}}_T : t = 0\}$.

Theorem 4.4 *Suppose that Assumption 3.2, (H1), (H2) and (H3) are satisfied. Let $\rho \in L^\infty(\mathcal{D})$ be a continuously differentiable probability measure bounded by a positive constant from below. Assume that $u \in C^{2,1}(\bar{\mathcal{D}}_T) \cap C(\bar{\mathcal{D}}_T)$ satisfies (3.19) subject to initial data (3.16) and boundary conditions (3.18). Then,*

$$\min_{\bar{\mathcal{D}}_T} u = \min_{\Gamma \cup \mathcal{A}_1} u \quad \text{and} \quad \max_{\bar{\mathcal{D}}_T} u = \max_{\Gamma \cup \mathcal{A}_2} u. \quad (4.7)$$

In particular, $u(x, t) \in [-1, 1]$ for all $(x, t) \in \bar{\mathcal{D}}_T$, provided $u(x, 0) \in [-1, 1]$ for all $x \in \mathcal{D}$.

Proof. Consider the operator $Lu = \gamma\sigma_\eta \nabla \cdot (\rho^2 \nabla u)$. Then, $\rho\partial_t - L$ is a uniformly parabolic operator by the assumptions on ρ . The PDE (3.19) can be written as $\rho\partial_t u - Lu = -\kappa\rho W'(u)$. For $(x, t) \in \mathcal{B}_1 = \{(x, t) \in \mathcal{D}_T : u(x, t) < -1\}$, we have $\rho\partial_t u - Lu \geq 0$ and $\min_{\bar{\mathcal{B}}_1} u(x, t)$ is attained on $\bar{\mathcal{B}}_1 \setminus \mathcal{B}_1 = \{(x, t) \in \bar{\mathcal{B}}_1 : t = 0\} \cup \{u = -1\}$ by the weak maximum principle [7, §7.1.4, Theorem 8]. Similarly, for $\mathcal{B}_2 = \{(x, t) \in \mathcal{D}_T : u(x, t) > 1\}$, we have $\rho\partial_t u - Lu \leq 0$ and $\max_{\bar{\mathcal{B}}_2} u(x, t)$ is attained on $\bar{\mathcal{B}}_2 \setminus \mathcal{B}_2 = \{(x, t) \in \bar{\mathcal{B}}_2 : t = 0\} \cup \{u = 1\}$. Since $u = -1$ on \mathcal{A}_1 and $u = 1$ on \mathcal{A}_2 by (3.18) for non-empty sets $\mathcal{A}_1, \mathcal{A}_2$, defined in Assumption 3.2, we can conclude that the minimum of u is attained on $\Gamma \cup \mathcal{A}_1$ and the maximum of u is attained on $\Gamma \cup \mathcal{A}_2$ which yields (4.7). \square

Note that the requirement that ρ is continuously differentiable is not restrictive for the maximum principle in Proposition 4.4 since properties of strong solution $u \in C^{2,1}(\mathcal{D}_T) \cap C(\bar{\mathcal{U}}_T)$ of (3.19) are described.

4.4. Dependence on edge weights and regularization. We conclude by studying the behavior of solutions with respect to the edge weights w_{ij} and the regularization parameter κ . The definition of σ_η in (3.1) suggests that for $\eta \leq \tilde{\eta}$ we have $\sigma_\eta \leq \sigma_{\tilde{\eta}}$. In particular, for $\eta(s) = \mathbb{1}_{[0,R]}(s)$ the constant σ_η increases as R increases. Since σ_η only arises as a multiplicative constant in (3.19), the prefactor $\gamma\sigma_\eta$ can be considered as rescaling in time. It is therefore sufficient to investigate the dependence of $\alpha > 0$ in

$$\rho\partial_t u = \nabla \cdot (\rho^2 \nabla u) - \alpha\rho W'(u), \quad x \in \mathcal{D},$$

where α decreases as σ_η increases. In the limit $\alpha \rightarrow 0$ its solution is equivalent to the solution of (3.19) for $\kappa = 0$ up to rescaling in time. For $\alpha \rightarrow \infty$, or equivalently $\kappa \rightarrow \infty$ in (3.19) we obtain a Γ -convergence result (again up to a rescaling in time). In doing so we define $\mathcal{F}_{\kappa_n} : L^1(\mathcal{D}) \rightarrow \mathbb{R} \cup \{+\infty\}$ for $n \in \mathbb{N}$ by

$$\mathcal{F}_{\kappa_n}(u) = \begin{cases} \frac{\gamma\sigma_\eta}{2\kappa_n} \int_{\mathcal{D}} \rho^2 |\nabla u|^2 dx + \kappa_n \int_{\mathcal{D}} \rho W(u) dx, & u \in L^4(\mathcal{D}) \cap H^1(\mathcal{D}), \\ +\infty, & \text{otherwise.} \end{cases}$$

Here, the first case is equivalent to \mathcal{E} in (3.20) when replacing κ by κ_n and rescaling the functional. Minimizers of \mathcal{F}_{κ_n} are expected to be indicator functions taking values in $\{-1, 1\}$. The rescaling by $1/\kappa_n$ in the first term of \mathcal{F}_{κ_n} ensures that the energy is finite. Note that the corresponding term in the original energy (3.20), blows up for all non-constant indicator functions.

We denote by $\text{BV}(\mathcal{D}; \{-1, 1\})$ the space of functions of bounded variation with values in $\{-1, 1\}$. For the ease of notation, we set $\sigma_W = \int_{-1}^1 \sqrt{W(s)} ds$ and introduce the weighted total variation

$$\text{TV}_\rho(u) = \sup \left\{ \int_{\mathcal{D}} u \text{div}(\rho^{\frac{3}{2}} \phi) dx : \phi \in C_c^\infty(\mathcal{D}; \mathbb{R}^d) \text{ s.t. } \|\phi\|_\infty \leq 1 \right\}.$$

We define the Γ -limit $\mathcal{F} : L^1(\mathcal{D}) \rightarrow \mathbb{R} \cup \{+\infty\}$ of \mathcal{F}_{κ_n} by

$$\mathcal{F}(u) = \begin{cases} \sqrt{2\gamma\sigma_\eta} \sigma_W \text{TV}_\rho(u), & u \in \text{BV}(\mathcal{D}; \{-1, 1\}), \\ +\infty, & \text{otherwise.} \end{cases}$$

This functional is motivated by the following observation: for $u \in W^{1,2}(\mathcal{D})$ and $f(t) = \int_{-1}^t \sqrt{W(s)} ds$ with $t \in \mathbb{R}$ we have that $\nabla(f \circ u) = \sqrt{W(u)} \nabla u$. Therefore

$$\begin{aligned} \frac{\gamma\sigma_\eta}{2\kappa_n} \int_{\mathcal{D}} \rho^2 |\nabla u|^2 dx + \kappa_n \int_{\mathcal{D}} \rho W(u) dx &\geq \sqrt{2\gamma\sigma_\eta} \int_{\mathcal{D}} \rho^{\frac{3}{2}} |\nabla(f \circ u)| dx \\ &= \sqrt{2\gamma\sigma_\eta} \text{TV}_\rho(f \circ u). \end{aligned}$$

On the other hand $u \in \text{BV}(\mathcal{D}; \{-1, 1\})$ implies $\text{TV}_\rho(f \circ u) = \sigma_W \text{TV}_\rho(u)$ since $f \circ u = f(-1)\chi_{\{u=-1\}} + f(1)\chi_{\{u=1\}} = \sigma_W \chi_{\{u=1\}}$.

Theorem 4.5 *Let $\rho \in C^1(\mathcal{D})$ be a probability measure on \mathcal{D} which is bounded from below by a positive constant and let $\{\kappa_n\}$ be a non-negative, diverging sequence. Furthermore let (H1) and*

(H2) be satisfied.

Then, \mathcal{F}_{κ_n} Γ -converges to \mathcal{F} as $n \rightarrow \infty$. Moreover, there exists a minimizer of \mathcal{F} in $L^1(\mathcal{D})$ and

$$\min\{\mathcal{F}(u) : u \in L^1(\mathcal{D})\} = \liminf_{n \rightarrow \infty} \{\mathcal{F}_{\kappa_n}(u) : u \in L^1(\mathcal{D})\}.$$

If $\{u_{\kappa_n}\} \subset L^1(\mathcal{D})$ is a precompact sequence such that

$$\lim_{n \rightarrow \infty} \mathcal{F}_{\kappa_n}(u_{\kappa_n}) = \liminf_{n \rightarrow \infty} \{\mathcal{F}_{\kappa_n}(u) : u \in L^1(\mathcal{D})\},$$

then every cluster point of this sequence is a minimizer of \mathcal{F} .

Proof. By [2, Theorem 1.21], it is sufficient to show Γ -convergence and the compactness property for \mathcal{F}_{κ_n} , i.e. that any sequence $\{u_{\kappa_n}\}$ for which \mathcal{F}_{κ_n} is uniformly bounded has a convergent subsequence. Since ρ is bounded from above and below by positive constants, the compactness property of \mathcal{F}_{κ_n} follows immediately from the compactness property of the Ginzburg-Landau functional $\mathcal{F}_{\varepsilon}^{GL} : L^1(\mathcal{D}) \rightarrow \mathbb{R}$, defined as

$$\mathcal{F}_{\varepsilon}^{GL}(u) = \begin{cases} \int_{\mathcal{D}} \varepsilon |\nabla u|^2 + \frac{1}{\varepsilon} W(u) \, dx, & u \in W^{1,2}(\mathcal{D}), \\ \infty, & \text{otherwise} \end{cases} \quad (4.8)$$

for $\varepsilon > 0$ [15, 16, 14, 20]. The proof of the Γ -convergence of (4.8) to

$$\mathcal{F}^{GL}(u) = \begin{cases} 2\sigma_W \text{TV}(u, \mathcal{D}), & u \in \text{BV}(\mathcal{D}; \{-1, 1\}), \\ \infty, & \text{otherwise,} \end{cases}$$

as $\varepsilon \rightarrow 0$, cf. [15, 16], can be adapted to include the weight $\rho^{\frac{3}{2}}$. \square

5. NUMERICS

We conclude by illustrating the dynamics of solutions with computational experiments. We start by discussing the respective numerical schemes on the micro- and the macroscopic level, before investigating the consistency across levels, the impact of the initial conditions as well as the sensitivity with respect to the model parameters.

5.1. Numerical methods.

5.1.1. The microscopic solver. The microscopic simulations are based on an explicit in time discretisation of (2.2). Given the distribution of points $X_i \in \mathbb{R}^d$, $i = 1, \dots, n + m$ the respective weights w_{ij} are computed using

$$w(z) = \mathbb{1}_{\|z\| \leq R},$$

for a suitably chosen interaction radius $R > 0$. At first we consider the case of two labels. Let u_i^k denote the label of point X_i at time $t^k = k\Delta t$, where Δt is the discrete time step. To set the initial condition $u_i^0 := u_i(0)$ we assign the value 1 or -1 to correctly labeled points and choose one of the following three options for the remaining points:

- (1) $u_i^0 = 0$ for all $i = 1, \dots, n$.
- (2) $u_i^0 = \mathcal{U}([-1, 1])$, where \mathcal{U} is the uniform distribution on $[-1, 1]$.
- (3) $u_i^0 = \mathcal{N}(0, \sigma^2)$, where \mathcal{N} denotes the normal distribution with mean 0 and variance σ^2 .

Note that setting the boundary conditions to a non-zero value, introduces a bias towards a specific label. While in 1 no prior knowledge about the distribution of labels is imposed, settings 2 and 3 specify a prior weighting of labels in one direction or another. Labels are then updated by the explicit discretisation of (2.2):

$$u_i^{k+1} = u_i^k + \frac{\gamma \Delta t}{n + m} \sum_{j=1}^{n+m} w_{ij} (u_j^k - u_i^k) - \kappa \Delta t W'(u_i^k). \quad (5.1)$$

Recall that W is a double well potential, which enforces binary labels ± 1 . Note that in contrast to the macroscopic setting already labeled points X_i , $i = n, \dots, n + m$, can be located in the interior as well as the exterior of the computational domain.

In the case of k labels we use one-hot encoding and consider a binary vector valued function

$u_i(t) = (u_{i,1}(t), \dots, u_{i,k}(t))$ instead. The components of the vector u_i take values in $[0, 1]$ - these values can be interpreted as the probability that the point is assigned to the respective label. Labels are updated as in (5.1), using a potential W with minima at 0 and 1. As a natural next step one would consider an additional regularization term to enforce sparse labeling. We leave this point for future investigation.

5.1.2. The macroscopic solver. The simulation of the macroscopic model (3.19) for a given point cloud requires several pre-processing steps. First the calculation of the computational domain, which corresponds to the convex hull of V . We assume that for each label at least two neighboring vertices are correctly labeled. We set Dirichlet boundary conditions on the boundary edge connecting the two, while assuming Neumann boundary conditions on the rest of the domain. In case of binary labels we either set ± 1 , while we assign a value to each label for k labels and adjust the potential W accordingly. Next we calculate the respective particle density using Gaussian kernels

$$\eta_\varepsilon(x) = ((2\pi)^k |\Sigma|)^{-\frac{1}{2}} e^{-\frac{1}{2} x^T \Sigma^{-1} x} \text{ with } \Sigma = \text{diag}(\varepsilon, \dots, \varepsilon)$$

Equation (3.19) is then solved using a splitting scheme, in which we first perform an implicit in time step for the diffusive part followed by an explicit in time step of the nonlinear reaction term. We use a finite difference discretization in 1D and a finite element method in 2D for each splitting step.

5.2. Computational experiments. For the computational experiments of the one-dimensional microscopic problem (2.2) with discretization (5.1), we consider $n = 250$ data points in the one-dimensional setting and parameters $\gamma = 250$ and $\kappa = 0.25$, unless stated otherwise. We generate the underlying point cloud by sampling $n/2$ points from $\mathcal{N}(-0.25, 0.125)$ and $n/2$ points from $\mathcal{N}(0.4, 0.1)$. For the weights, we consider $w_{ij} = \mathbb{1}_{[0,R]}(|X_i - X_j|)$ with $R = 0.25$.

Dependence on the initial data. To investigate the dependence on the initial data, we consider a homogeneous distribution as in case 1, uniformly distributed points as in 2 or normally distributed ones with standard deviation 0.1 as in case 3. The respective final label distribution is shown in Figure 2, in which we use the following color coding: green corresponds to unbiased labels, that is $u_i = 0$, while blue and orange encode positive or negative values of u_i . As also shown in Proposition 3.1, the energy decays independent of the choice of initial data. While a separation into two clusters always occurs for homogeneous initial data as in Figure 2(A), the bias in the randomly normally or uniformly distributed case may result in one large cluster and a second cluster consisting only of the labeled data point at the boundary, see Figure 2(B). Moreover, the bias in the initial data may result in multiple clusters with small clusters of the labeled points on the boundary as in Figure 2(C). We have seen that the random allocation of initial labels may lead to incorrect classifications. However, if the random initial label distribution is close to the truth, then the algorithm identifies the two clusters correctly, see Figure 2(D). This observation leads to interesting questions about the dependence of solutions on the initial datum.

Dependence of the label location. For the homogeneous initial data 1, we consider different label locations of the labeled data points in Figure 3. We observe that the labeling fails in the case of mislabeled points, see Figure 3(A). However, if the given labels are assigned correctly, clusters may be identified correctly even if the points are located in the interior of the point cloud, see Figure 3(B).

Dependence on the scaling parameters γ and κ . As outlined in Section 4.4, the scaling parameters γ and κ can be regarded as rescaling in time. Hence it is sufficient to consider $\gamma = 1$, $\sigma_\eta = \frac{1}{2} \int_{\mathbb{R}} \eta(|x|) |x \cdot e|^2 dx = 0.03125$ by (3.1) for $\eta(s) = \mathbb{1}_{[0,R]}(s)$ with $R = 0.25$ and vary κ only. Since Section 4.4 investigates the large data limit $n \rightarrow \infty$, we consider solutions of the macroscopic model (3.19) in the following. Figure 4 illustrates the solution to (3.19) for $\kappa = 0$ and $\kappa = 100$ for given data distributions ρ and homogeneous initial data. As shown in Section 4.4, the solution approximates an indicator function for strictly positive functions ρ . Note that the solutions of the microscopic and macroscopic model are consistent due to the derivation of the limit in Section 3.3 and numerical examples are also included in Figure 5.

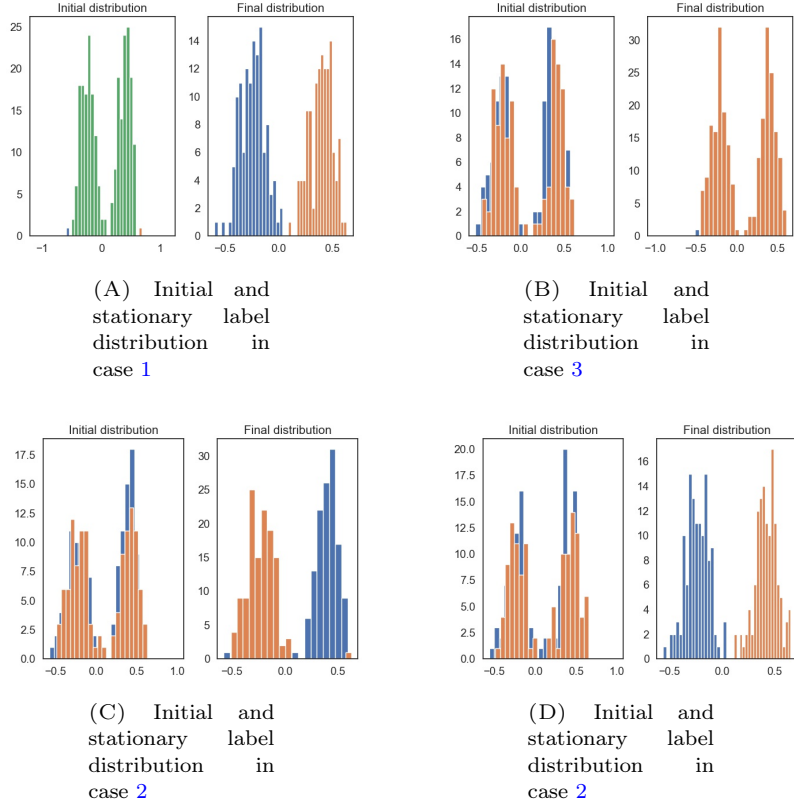


FIGURE 2. Dependence on initial data for different initial distributions and their stationary solution for the microscopic discretisation (5.1).

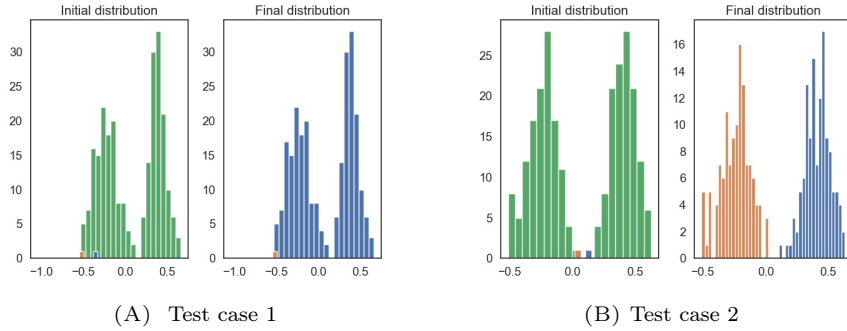


FIGURE 3. Dependence on label location for initial distribution 1 and their stationary solution for the microscopic discretisation (5.1).

Consistency of the microscopic and the macroscopic model. In the following we will investigate the consistency of the micro- and macroscopic model with 1D and 2D examples.

1D. We wish to compare the behavior of the microscopic and macroscopic solver for varying κ . In doing so we consider the original microscopic label distribution of 250 points equally distributed between two Gaussians. The respective density is also shown in Figure 4(A). To compare the results of the macroscopic discretisation in Figure 4(A) to the microscopic discretisation (5.1), we

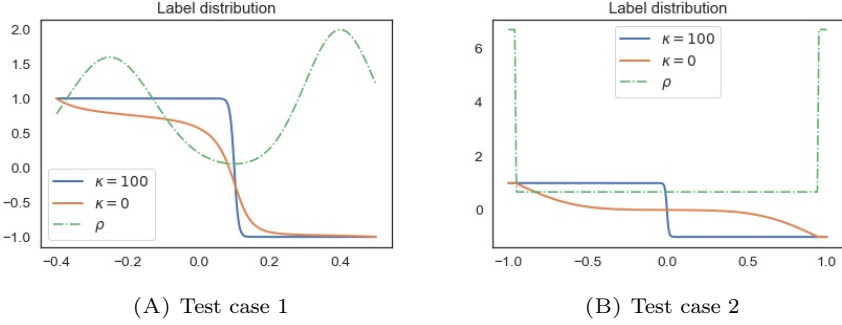


FIGURE 4. Stationary solution for the macroscopic discretisation for $\kappa = 0$ and $\kappa = 100$ for different densities ρ and homogeneous initial data 1.

consider homogeneous initial data 1, set $\gamma = 1$ and vary κ in Figure 5. We observe a very good agreement of the two levels.

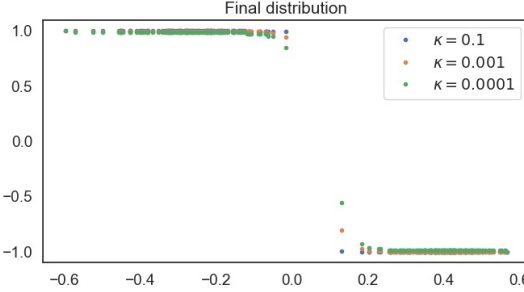


FIGURE 5. Stationary solution for the microscopic discretisation (5.1) for different κ and homogeneous initial data 1.

Two moons. Next we investigate the performance of the microscopic and macroscopic solver for the well-known two moons problem. In doing so we generate a noisy two moon dataset of 500 points using Scikit, cf. [18] with standard deviation 0.1. We assume that the labels of points defining the convex hull of the dataset are known and set the labels of all other points to 0. Figure 6 shows the initial as well as final label distribution at time $T = 25$ using the parameters $\gamma = 1.0$ and $\kappa = 10$. The final distribution for the microscopic and macroscopic models in shown in Figure 7.

Multilabel and more complex labeling problems. We conclude by comparing the performance of the proposed label propagation to classify single digits in the National Institute of Standards and Technology (NIST) dataset. In doing so we use the digits dataset of the Scikit-learn project, see [18]. It consists of 1797 samples of digital digits, which were extracted and pre-processed from the NIST dataset. Each sample corresponds to an 8×8 image of a digit taking values in $I = \{0, 1, \dots, 16\}$. We wish to assign each image to one of the numbers in $L = \{0, \dots, 9\}$.

We use the Wasserstein distance $d_{\mathcal{W}_2}$ to compare images $X_i \in I^8 \times I^8$ using the Python optimal transport (POT) library, see [8] and [19] for more information on computational optimal transport. The weights are then set to

$$w_{ij} = \mathbb{1}_{d_{\mathcal{W}_2}(X_i, X_j) \leq \bar{c}} d_{\mathcal{W}_2}(X_i, X_j)^{-1}.$$

Images are only connected if their Wasserstein distance is below a certain threshold \bar{c} . Then the respective weight corresponds to the inverse of the Wasserstein distance. We randomly choose 320 samples, calculate the respective weight matrix and assume that the first 40 digits are correctly labelled. The remaining labels are then computed using (2.1). To assign the images to the different

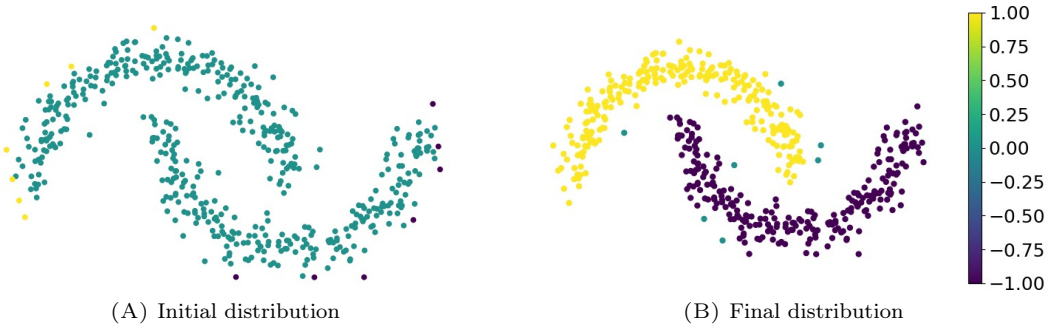


FIGURE 6. Initial and final distribution at $T = 25$ using the parameters $\gamma = 1.0$ and $\kappa = 10$. We assume that all points defining the convex hull are correctly labelled.

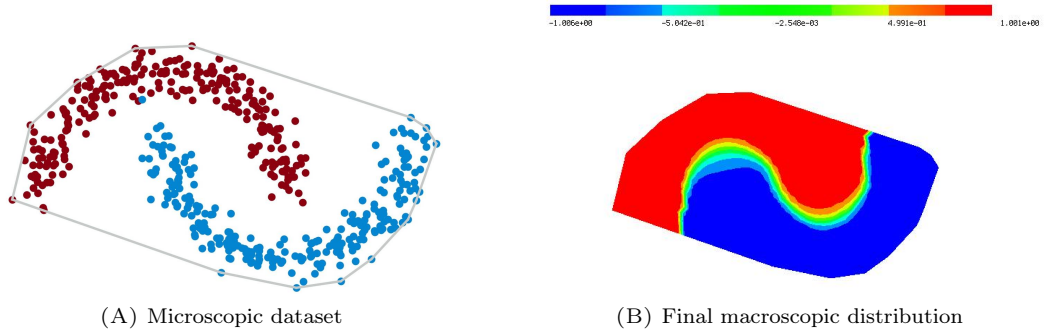


FIGURE 7. Final distribution at $T = 25$ using the parameters $\gamma = 1.0$ and $\kappa = 10$ for the microscopic and macroscopic models. We assume that all points defining the convex hull are correctly labelled.

labels, we use one-hot encoding - hence u_i is a vector valued function in \mathbb{R}^{10} . Labels take values in the interval $[0, 1]$, which can be interpreted as the probability that the image corresponds to the respective number in L . In this case the double well potential W has to be changed accordingly - with two wells located at $x = 0$ and $x = 1$, in particular $W(x) = x^2(x - 1)^2$.

The performance of the algorithm depends strongly on the cut-off \bar{c} . We set it to one-tenth the value of the maximum Wasserstein distance:

$$\bar{c} = 0.1 \times \max_{i,j \in \{1, \dots, 320\}} w_{ij}$$

choose $\gamma = 1$ and $\kappa = 10$. We compare the maximum entry of each vector u_i , $i = 1, \dots, 320$ at time $T = 20$ with the respective correct labels - managing to assign 84.285% of the labels correctly. We believe that the performance of the scheme can be improved by fine-tuning the parameters and adding regularization terms to enforce sparsity of the vector u_i . This is however beyond the scope of this work, in which we wish to demonstrate the general feasibility of the proposed approach.

ACKNOWLEDGMENTS:

LMK acknowledges support from the European Union Horizon 2020 research and innovation programmes under the Marie Skłodowska-Curie grant agreement No. 777826 (NoMADS) and No. 691070 (CHIPS), the Cantab Capital Institute for the Mathematics of Information and Magdalene College, Cambridge (Nevile Research Fellowship). MTW acknowledges partial support from

the Austrian Academy of Sciences under the New Frontier's grant NST-0001. Both authors acknowledge support of the Warwick Research Development Fund through the project 'Using Partial Differential Equations Techniques to Analyse Data-Rich Phenomena'.

REFERENCES

- [1] A. L. Bertozzi and A. Flenner. Diffuse interface models on graphs for classification of high dimensional data. *Multiscale Modeling & Simulation*, 10(3):1090–1118, 2012.
- [2] A. Braides. *Gamma-convergence for Beginners*. Oxford Lecture Series in Mathematics. Oxford University Press, 2002.
- [3] J. A. Carrillo, Y.-P. Choi, and S. P. Perez. A review on attractive–repulsive hydrodynamics for consensus in collective behavior. In *Active Particles, Volume 1*, pages 259–298. Springer, 2017.
- [4] F. Cucker and S. Smale. Emergent behavior in flocks. *IEEE Transactions on automatic control*, 52(5):852–862, 2007.
- [5] B. Düring, C. Gottschlich, S. Huckemann, L. Kreusser, and C.-B. Schönlieb. An anisotropic interaction model for simulating fingerprints. *Journal of Mathematical Biology*, 78, 11 2017.
- [6] B. Düring, P. Markowich, J.-F. Pietschmann, and M.-T. Wolfram. Boltzmann and Fokker–Planck equations modelling opinion formation in the presence of strong leaders. *Proceedings of the Royal Society A: Mathematical, Physical and Engineering Sciences*, 465(2112):3687–3708, 2009.
- [7] L. C. Evans. *Partial Differential Equations*. Grad. Stud. Math. Amer. Math. Soc., Providence, R.I., 2010.
- [8] R. Flamary and N. Courty. POT Python Optimal Transport library, 2017.
- [9] Y. van Gennip and A. L. Bertozzi. Γ -convergence of graph Ginzburg–Landau functionals. *Adv. Differential Equations*, 17(11/12):1115–1180, 11 2012.
- [10] J. Haskovec. Flocking dynamics and mean-field limit in the cucker–smale-type model with topological interactions. *Physica D: Nonlinear Phenomena*, 261:42 – 51, 2013.
- [11] F. Hoffmann, B. Hosseini, A.A. Oberai, and A.M. Stuart. Spectral analysis of weighted Laplacians arising in data clustering, 2019.
- [12] U. Krause. A discrete nonlinear and non-autonomous model of consensus formation. *Communications in difference equations*, 2000:227–236, 2000.
- [13] E. Merkurjev, T. Kostic, and A. L. Bertozzi. An MBO scheme on graphs for classification and image processing. *SIAM Journal on Imaging Sciences*, 6(4):1903–1930, 2013.
- [14] L. Modica. The gradient theory of phase transitions and the minimal interface criterion. *Arch. Rational Mech. Anal.*, 98:123–142, 1987.
- [15] L. Modica and S. Mortola. Il limite nella Γ -convergenza di una famiglia di funzionali ellittici. *Boll. Un. Mat. Ital. A (5)*, 14(3):526–529, 1977.
- [16] L. Modica and S. Mortola. Un esempio di Γ -convergenza. *Boll. Un. Mat. Ital. B (5)*, 14(1):285–299, 1977.
- [17] S. Motsch and E. Tadmor. Heterophilious Dynamics Enhances Consensus. *SIAM Review*, 56(4):577–621, 2014.
- [18] F. Pedregosa, G. Varoquaux, A. Gramfort, V. Michel, B. Thirion, O. Grisel, M. Blondel, P. Prettenhofer, R. Weiss, V. Dubourg, J. Vanderplas, A. Passos, D. Cournapeau, M. Brucher, M. Perrot, and E. Duchesnay. Scikit-learn: Machine learning in Python. *Journal of Machine Learning Research*, 12:2825–2830, 2011.
- [19] G. Peyré, M. Cuturi, et al. *Computational Optimal Transport: With Applications to Data Science*, volume 11. Now Publishers, Inc., 2019.
- [20] P. Sternberg. The effect of a singular perturbation on nonconvex variational problems. *Arch. Rational Mech. Anal.*, 101:209–260, 1988.
- [21] N. G. Trillos and D. Slepčev. A variational approach to the consistency of spectral clustering. *Applied and Computational Harmonic Analysis*, 45(2):239–281, 2018.
- [22] X. Zhu and Z. Ghahramani. Learning from unlabeled data with label propagation. Technical report, Carnegie Mellon, 2002.
- [23] X. Zhu, Z. Ghahramani, and J. D Lafferty. Semi-supervised learning using gaussian fields and harmonic functions. In *Proceedings of the 20th International conference on Machine learning (ICML-03)*, pages 912–919, 2003.

LISA MARIA KREUSSER, DEPARTMENT FOR APPLIED MATHEMATICS AND THEORETICAL PHYSICS, UNIVERSITY OF CAMBRIDGE, WILBERFORCE ROAD, CAMBRIDGE CB3 0WA, UK

MARIE-THERESE WOLFRAM, MATHEMATICS INSTITUTE, UNIVERSITY OF WARWICK, CV47AL COVENTRY, UK AND RICAM, AUSTRIAN ACADEMY OF SCIENCES, ALtenbergerstr. 69, 4040 LINZ, AUSTRIA